Hindawi
Advances in Civil Engineering
Volume 2019, Article ID 5173132, 11 pages
https://doi.org/10.1155/2019/5173132

Research Article

Bridge Structure Dynamic Analysis under Vessel Impact Loading considering Soil-Pile Interaction and Linear Soil Stiffness Approximation

Jingfeng Zhang,[1] **Xiaozhen Li**,[2] **Yuan Jing**,[1] **and Wanshui Han**[1]

[1]*School of Highway, Chang'an University, Xi'an, Shaanxi, China*
[2]*School of Civil Engineering, Southwest Jiaotong University, Chengdu, Sichuan, China*

Correspondence should be addressed to Jingfeng Zhang; jfzhang@chd.edu.cn

Received 9 August 2018; Accepted 27 January 2019; Published 17 March 2019

Academic Editor: Dong Zhao

The appropriate modeling of the soil-pile interaction (SPI) is critical to get the reasonable dynamic responses of bridge structure under impact loading. Of various SPI modeling approaches, utilizing *p-y* and *t-z* curves is a common method to represent the nonlinear lateral resistance and skin friction of pile-surrounding soil. This paper accomplished SPI modeling for the bridge pylon impact analysis with compression-only nonlinear springs and linear dashpots. The kinematic interaction and pile group effect were incorporated into the SPI. A variety of pylon impact analyses were conducted under energy-variation impact loads. The structure dynamic responses were compared and discussed considering the influences of pile group effect, soil damping, and axial *t-z* spring. An approximate approach was proposed to derive the linearized stiffness of soil for the purpose of engineering calculation. It was concluded from the extensive simulations that the impact load generated from higher initial energy induced more significant structural responses and larger soil inelastic deformation than smaller initial energy. The piles in the leading row possessed larger bending moments, whereas they exhibited smaller pile deformation than the responses of trailing row piles. Soil damping applied in SPI played positive roles on the reduction of structural responses. Replacing the *t-z* spring by fixing the degree-of-freedom (DOF) in the vertical direction was capable to yield satisfactory results of structural responses. The proposed linear soil stiffness was demonstrated to be applicable in the SPI modeling of structure impact analysis.

1. Introduction

Catastrophic accidents from the vessel-bridge collisions have raised concerns about the bridge safety under impact loading. Design methods and protective measures of bridge structures under vessel impact action get a lot of attention from engineers and researchers in recent years [1–3]. The static equivalent vessel impact forces were recommended in the design codes and specifications of many countries and communities [4–7]. However, previous studies had shown that the vessel-bridge collision is a dynamic interaction process, and the dynamic analysis approach should be adopted to accurately quantify the bridge responses due to impact action [8–10]. In the structure dynamic analysis under vessel impact load, the impact responses of the whole bridge structure, especially for the substructure, were strongly influenced by soil-pile interaction (SPI) [11, 12]. It is necessary to take the SPI into account for obtaining reasonable bridge dynamic responses [13].

There are several alternative methods to accomplish SPI in the bridge foundation modeling for structure dynamic analysis. The soil continuum assumption based on elastic mechanics is often employed to investigate the soil resistance to piles while sometimes it is difficult to consider the nonlinear soil properties in the analysis process [14, 15]. With the development of the computer technique, the finite element method (FEM) and boundary element method (BEM) are used to model the SPI for structure analysis [16, 17]. However, the analysis approaches of FEM and BEM are not suitable to be adopted in the preliminary design stage of the bridge structures due to its time-consuming and the complicated settings in computation. Based on the Winkler

foundation theory, the surrounding soil also can be discretized into a series of springs to represent its resistance. Springs are assumed along the pile length due to its clear physical concept and convenience in application (sometimes working in coordination with the damping dashpots), which has become a common approach to simulate the pile-surrounding soil in the engineering practice.

The SPI modeling approach based on Winkler foundation theory can be classified into two categories according to the features of soil stiffness. The first approach is that the soil deformation behavior is assumed as elastic, and the soil spring has a constant stiffness. Various methods recommended in the structure design codes, such as "*m*-method" and "*k*-method," are adopted in the engineering application [9, 18]. Since the constant stiffness assumption ignored the soil inelastic deformation behavior and may not be applicable under dramatic lateral loading such as earthquake and vessel impact, the *p-y* curve for soil lateral resistance and *t-z* curve for the soil-pile skin friction are more appropriate in the SPI simulation in this study [19].

In the structural dynamic analysis considering SPI, the soil resistance consists of two individual parts: (1) the displacement-dependent spring force and (2) the velocity-dependent damping force [11], whereas the traditional static *p-y* curve ignored the resistance contribution by the rate-dependent effect and may underestimate the soil resistance. Moreover, in a pile group foundation, the leading piles may "shade" the subsequent trailing piles which leads to less resistance compared with the sum of the single pile resistance. It is necessary to consider the various soil resistances for the piles in different rows of pile group foundation. Although the *p-y* soil curve shows advantages in the modeling of soil resistance, linear stiffness of the soil resistance is still preferred in the engineering practice and reasonable approximation is in great demand to get the linear stiffness from the *p-y* soil curve.

In this paper, the soil-pile interaction (SPI) was considered in the pile group foundation modeling of cable-stayed bridge pylon. A variety of bridge pylon impact analyses were conducted when subjected to energy-variation impact loads. The influences of pile group effect, soil damping, and axial *t-z* spring were compared and discussed on the structure and soil responses. An equivalent linear soil stiffness approximation method is proposed and validated for the purpose of engineering application.

2. Finite Element Modeling of Soil-Structure Interaction

2.1. Finite Element Modeling of Bridge Pylon. Cable-stayed bridge, with superior spanning ability, is frequently built over the inner river navigation channel and near-sea area. In the life cycle of a cable-stayed bridge, ensuring the safety of the bridge pylon under the accidental action, such as vessel collision, is of prime importance to the overall structure. It is required to consider vessel collision action in the design of cable-stayed bridge. Therefore, a cable-stayed bridge pylon with elevated cap-pile group foundation was taken as an example to conduct the dynamic analysis under vessel impact in this study.

The clear height of the bridge pylon employed in this study is 190.5 m, and the thickness of the cap is 9.5 m. A pile group foundation consisting of 15 cast-in-situ bored piles will support the vertical load and the lateral load. The length of each pile is 42.5 m. The detailed configuration of the pylon is shown in Figure 1(a). The finite element (FE) model of bridge pylon was built for conducting the vessel-bridge transient impact analysis. The structure components above the cap, as well as the drilled pile, were modeled by using 2-node beam elements. The pylon cap was modeled with a concentrated mass which reflected its significant contribution to the total mass of the bridge pylon. This mass element was connected with the pylon and the piles with rigid coupling links (Figure 1(b)). The material model of structure was assumed to be elastic. The concrete density of pylon is 2550 kg/m^3, and Poisson's ratio is 0.2. Young's modulus for the pylon and the foundation are 3.55*E*4 MPa and 3.00*E*4 MPa, respectively.

2.2. p-y and t-z Curves for Surrounding Soil Resistances. The soil layer profile and its primary properties are shown in Figure 2. The soil layers are fine sand, soft clay, and moderately weathered sandstone from the top of the river bed to the pile tip, respectively. The surrounding soil along the pile length will provide vertical and lateral resistance for the pile group to support the whole structure.

Extensive work has been done to experimentally get the *p-y* curves for cohesionless sandy soils. Herein, the *p-y* curves for the 1st layer sand were developed according to the approach proposed by Reese et al. [20]. In the sand *p-y* curve, it usually consists of four segments as shown in equation (1). Except for the 2nd segment in the Reese's *p-y* curve expression presented as parabolic form, the other three parts are all expressed as linear forms:

$$p = \begin{cases} (kz)y, & \text{for } 0 \le y < y_{\mathrm{k}}, \\ p_{\mathrm{m}}\left(\dfrac{y}{y_{\mathrm{m}}}\right)^{1/n}, & \text{for } y_{\mathrm{k}} \le y < y_{\mathrm{m}}, \\ p_{\mathrm{m}} + \dfrac{p_{\mathrm{m}} - p_{\mathrm{u}}}{y_{\mathrm{m}} - y_{\mathrm{u}}}(y - y_{\mathrm{m}}), & \text{for } y_{\mathrm{m}} \le y < y_{\mathrm{u}}, \\ p_{\mathrm{u}}, & \text{for } y \ge y_{\mathrm{u}}, \end{cases} \tag{1}$$

where p is the soil resistance per unit length of pile, k is the subgrade modulus of sand, z is the depth under the subgrade surface (m), and y is lateral deflection of pile. The other undetermined parameters of $y_{\mathrm{k}}, y_{\mathrm{m}}, p_{\mathrm{m}}, y_{\mathrm{u}}, p_{\mathrm{u}}$ in equation (1) are related to sand properties of internal friction angle and unit weight. More detailed procedure to calculate these parameters and develop the sand *p-y* curve can be found in FHWA's COM624P manual by Wang and Reese [21].

The lateral resistance model for the 2nd layer soft cohesive soil is characterized by Matlock [22]. The *p-y* curve can be generated according to the following equation:

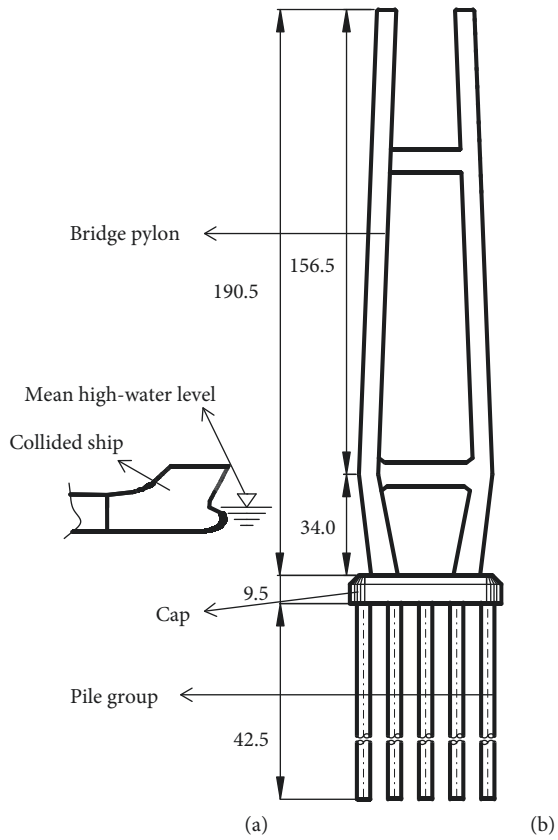

Figure 1: Bridge pylon structure. (a) Bridge pylon configuration. (b) FE model of bridge pylon.

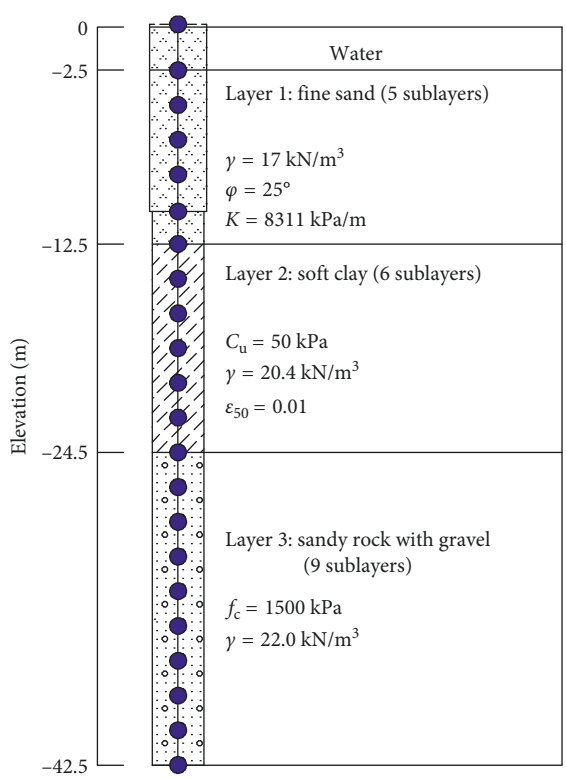

Figure 2: Soil profile and properties.

$$p = \begin{cases} 0.5p_{\mathrm{u}}\left(\dfrac{y}{y_c}\right)^{1/3}, & \text{for } \dfrac{y}{y_{50}} \le 8, \\ p_{\mathrm{u}}, & \text{for } \dfrac{y}{y_{50}} > 8, \end{cases} \tag{2}$$

where y_{50} is the deflection at 50% of the ultimate soil resistance strength and equals to $2.5\varepsilon_{50}D$. ε_{50} is the soil strain corresponding to one-half of the maximum stress in laboratory undrained compression tests. The ultimate lateral soil resistance of p_{u} can be calculated as

$$p_{\mathrm{u}} = \begin{cases} (3c_{\mathrm{u}} + \gamma' z)D + Jc_{\mathrm{u}}z, & \text{for } 0 < z < z_{R,\mathrm{soft}}, \\ 9c_{\mathrm{u}}D, & \text{for } z > z_{R,\mathrm{soft}}, \end{cases} \tag{3}$$

where γ' is the effective unit weight of soil in kN/m^3, c_{u} is the undrained shear strength of soil (kN/m^2), D is the pile diameter (m), J is a dimensionless empirical constant ranging from 0.25 to 0.50 with 0.5 recommended for soft normally consolidated clay, and $z_{R,\mathrm{soft}}$ is a transition depth below which the value of $(3c_{\mathrm{u}} + \gamma' z)D + Jc_{\mathrm{u}}z$ exceeds $9c_{\mathrm{u}}D$.

The p-y curve for the third medium weathered sandstone is based on the recommendation by McVay and Niraula [23]. The lateral resistance of sand rock, p, is considered as independent of the depth of covered soil. Two linear segments form the p-y relationship of sandstone. Normalizing

the p value (in kN/m) by $D^{0.85}q_u^{0.15}$, the sandstone p-y curve can be derived as

$$p = \begin{cases} 13750D^{0.85}q_u^{0.15}\left(\dfrac{y}{D}\right), & 0 < \dfrac{y}{D} < 0.004, \\ D^{0.85}q_u^{0.15}\left[1083\left(\dfrac{y}{D}\right) + 51\right], & 0.004 < \dfrac{y}{D} < 1, \end{cases} \quad (4)$$

where q_u is the unconfined compressive strength in kN/m^2.

2.3. Soil-Pile Interaction Modeling. Realizing the importance of the SPI to the responses of bridge substructure-subjected impact loading, the kinetic interaction between the pile and soil was accomplished including both the contributions of stiffness and damping. In the present study, the pile and the surrounding soil were discretized into 2 m equally from elevation −2.5 m down to the pile tips (Figure 2). At each elevation corresponding to the pile nodes, the soil lateral resistance was modeled by two perpendicular groups of nonlinear springs and dashpots, as shown in Figure 3. The nonlinear soil spring with the p-y curve was employed to represent the soil static stiffness under lateral loading. Moreover, since soil resistance increased significantly under dynamic loading, a linear dashpot element was set in parallel to the lateral p-y spring accounting for soil rate-dependent effect and radiation damping. The constant damping coefficient is related to wave propagation velocity in soil V and mass density of soil ρ, which can be determined by equation (5) according to the literature [24]. A is the surface area of pile that bears the induced force of damping dashpot. Assuming that the wave velocity V is equal to 70 m/s and ρ is 1700 kg/m^3, A is calculated by multiplying the sublayer depth of 2 m with the pile diameter of 3 m, which is equal to 6 m^2. The value of damping coefficient, c, is 714 kN/(m/s) in this study:

$$c = \rho V A. \quad (5)$$

In addition to the SPI in two perpendicular lateral directions, the axial soil resistance is of great significance for the pier to transfer lateral impact load to group-pile foundation. Conventional approach to model the axial SPI utilized t-z curves, and a nonlinear spring was placed at each pile node along the pile length (Figure 3). The pile bottom node was fixed rigidly to represent the rock-socketed effect.

2.4. Pile Group Effects. The lateral resistance of a single pile within a group is less than that of a single isolated pile, which is called "group effects." The common approach to account for this effect is to multiply the p in the p-y curve with a reduction factor called p-multiplier to scale down the soil resistance. In addition to the influence by pile spacing, the value of p-multiplier also depends on the pile position in the loading direction since the leading piles carry more load than the trailing piles. As shown in Figure 4, the 1st row piles acted as the leading pile in the positive movement direction, while these leading-row piles might transform into trailing-row piles as piles were moving back to the negative direction [11]. Therefore, the p-multipliers of piles were changing

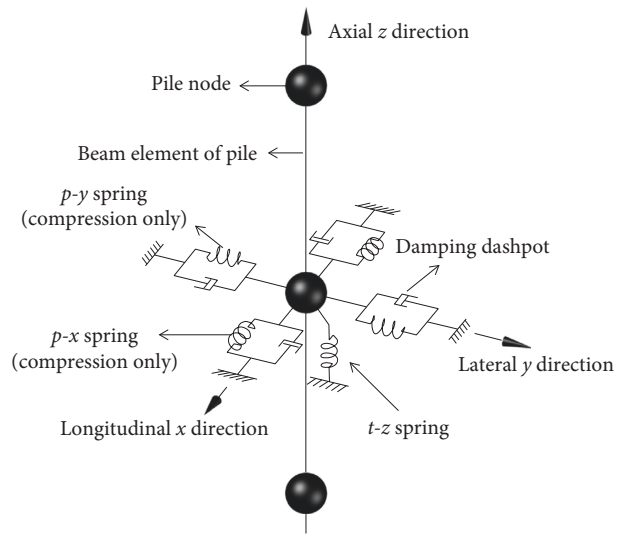

Figure 3: Schematic of SPI modeling.

depending on the direction of pile motion. The choice of "p-multiplier" in this study was based on the recommendations in AASHTO LRFD Bridge Design Specifications [25]. The p-multiplier of the 1st, 2nd, and the last remaining rows of piles are 0.7, 0.5, and 0.35, respectively.

3. Vessel Impact Loads for Various Impact Energies

A cargo ship collided with a rigid wall was simulated to get the impact load time history with the use of explicit dynamic FE software, LS-DYNA (Figure 5) [26]. Different levels of impact energy were simulated by adjusting the vessel tonnage m and its impact velocity V. Three cases, i.e., low-energy impact, medium-energy impact, and high-energy impact were taken to conduct the vessel-bridge pylon impact analysis. The specific impact parameters as well as the key features in impact loads are listed in Table 1. The impact forces with respect to the time and crush depth obtained from the FE analysis are presented in Figure 6.

From the impact loads shown in Figure 6 and the key features listed in Table 1, it can be observed that the peak impact force P_{max} increased with the vessel impact energy, as well as the impact load impulse (the area surrounded by the impact load time history). Higher impact energy also caused deeper and more severe vessel bow crush, which demonstrated that the vessel bow absorbed more energy in the high-energy impact process.

4. Structure Transient Impact Analysis

Structure impact analysis was conducted by applying the impact load obtained from Section 3 on the bridge pylon. For all impact cases, the input load was applied at the node of the pylon column which was above 23 m from the cap (Figure 1). Except for the soil damping considered in the SPI modeling, a global Raleigh damping with a ratio coefficient of 0.05 was applied for the structure. The peak responses might occur either at the impact loading phase or the 1st

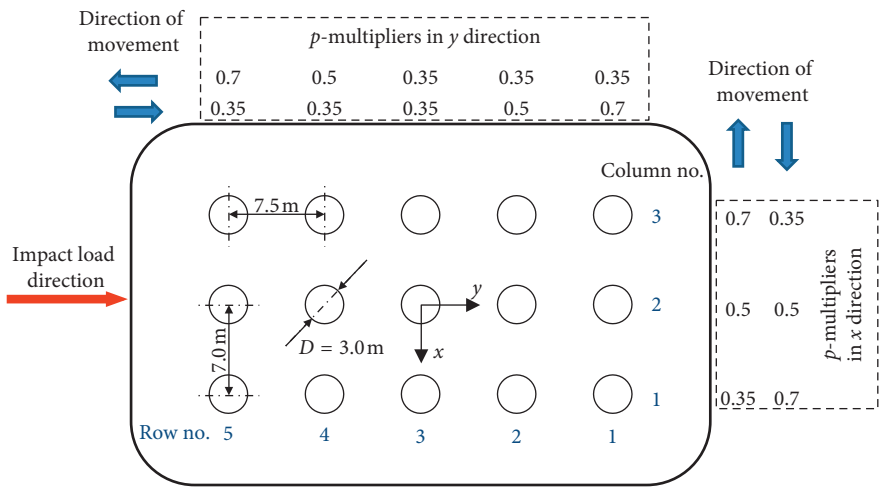

Figure 4: p-Multipliers in each row of the pile group.

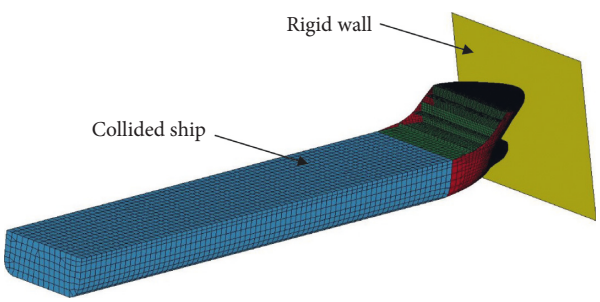

Figure 5: Vessel-rigid wall collision model.

Table 1: Impact parameters and load characteristics.

Impact cases	Vessel impact parameters		Load characteristics		
	m (t)	V (m/s)	P_{max} (MN)	Duration (s)	a_{max} (m)
Low energy	500	2	2.3	0.8	0.6
Medium energy	5000	2	10.9	2.3	2.9
High energy	5000	4	19.5	2.1	5.3

cycle of free vibration, and the simulation time should be long enough so that the peak responses could be captured. According to the 1st natural modal period of pylon (3.06 s) and the impact durations (≤2.3 s), the analysis duration was set to 8 s.

4.1. Pylon Dynamic Responses under Various Impact Loads. Dynamic analysis of bridge pylon was performed under the impact loads of low, medium, and high initial energies. As shown in Figure 7, it can be clearly found that the lateral displacements of both the cap and pylon top of high-energy impact were much larger than those of other two impact cases. The cap displacement was 6 cm approximately, and the pylon top displacement was nearly 16.5 cm from the high-energy impact.

To fully understand the pile deformation and soil resistance under various impact loads, the pile displacement in the 5th row of the pile group length at the cap maximum lateral deformation ($y_{max,cap}$) was given in Figure 8. The pile endured the largest lateral displacement under high-energy impact, and the maximum pile displacement 6 cm occurred at the top of pile. The maximum pile lateral displacements for medium- and low-energy impact cases were 2.2 cm and 0.6 cm, respectively.

Figure 9 displays the soil p-y curves of the 1st sublayer as the pile swayed to the positive direction. In the medium- and high-energy impact cases, the pile lateral displacement at the corresponding elevation of the 1st sublayer exceeded the soil elastic deformation limit $y_{el} = 0.009$ m and the surrounding soil went into the nonlinear deformation stage, while the displacement of pile in low-energy impact cases was less than the y_{el} that indicated the surrounded soil remained elastic. Except for the dynamic p-y curves obtained from the impact analysis, the static p-y curve was also presented for the purpose of comparison. It can be observed that significant differences existed between the dynamic p-y curves from impact analysis cases (especially for the medium- and high-energy impact) and static p-y curve. Soil resistance increased significantly owing to the incorporation of the linear dashpot accounting for the soil resistance rate-dependent increase. Larger velocity of pile movement excited by the impact load will lead to more significant increase on the soil resistance, as well as the loading stiffness of soil. As seen from Figure 9, the initial dynamic tangent stiffness k_0^d = 14044kN/m from the impact analysis was more than three times larger than the k_0^s = 4213kN/m of the static p-y curve. In general, considering the nonlinearity and rate-dependent increase on the resistance of soil is necessary for the dynamic analysis of pile that endures large lateral deformation.

4.2. Pile Dynamic Responses in Different Rows. Different p-multipliers were assigned to the p-y curves corresponding to piles in different rows according to Section 2.4, such that the deformation and inner forces of piles in each row might

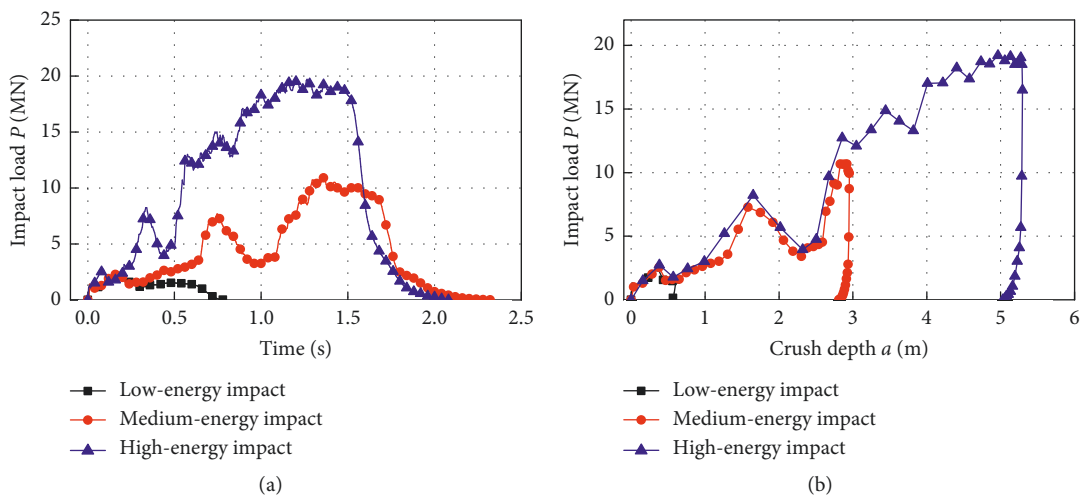

Figure 6: Impact load comparisons between the low- and high-energy impact. (a) Impact load time history. (b) Impact load versus crush depth.

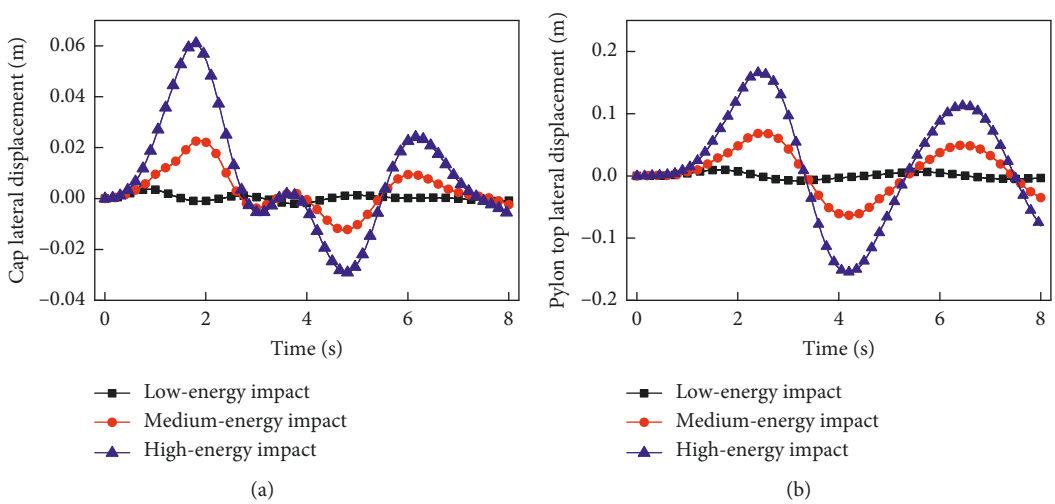

Figure 7: Bridge pylon lateral displacements under impact loads. (a) Cap lateral displacement. (b) Pylon top lateral displacement.

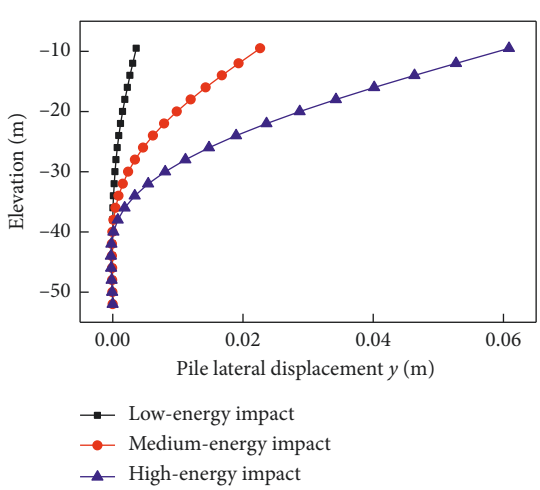

Figure 8: Pile lateral displacement in the 5th row.

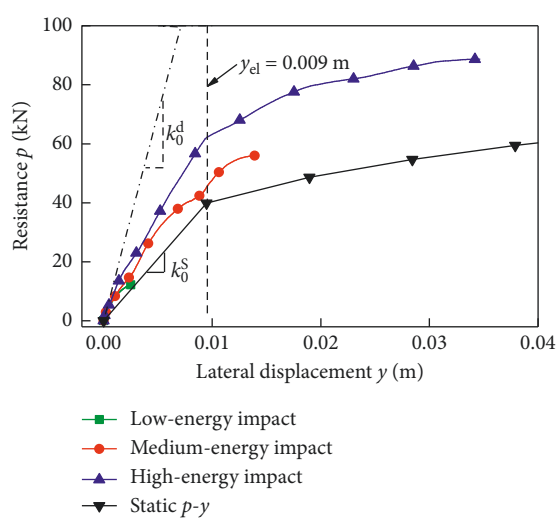

Figure 9: Soil p-y curves of the 1st sublayer.

exhibit distinctly. As the pylon cap reached its maximum positive displacement ($y_{max,cap}$), the 5th row piles had a little larger lateral deformation than the 1st row piles since the trailing 5th row piles had smaller p-multipliers than 1st row leading piles. While as the pile group moved back to minimum negative displacement ($y_{min,cap}$), the 1st row piles turned into trailing row piles such that the p-multipliers were changing accordingly. Therefore, slightly larger displacement was found in 1st row pile rather than 5th row piles at displacement of $y_{min,cap}$.

The percentages of the lateral load undertaken by piles in different rows are proportional to the stiffness. Thus, the leading rows which had larger p-multiplier engaged more to take the impact load. The bending moment of the pile shown in Figure 10(b) agreed well with this inference, which the 1st row at $y_{max,cap}$ and 5th row at $y_{min,cap}$ presented larger bending moments than 5th row at $y_{max,cap}$ and 1st row at $y_{min,cap}$, respectively.

4.3. Effect of Soil Damping on the Structural Responses. Rate-dependent soil resistance and energy dissipation within the soil influence the structure dynamic responses under impact loads significantly. Except for the viscous damping constant $c = \rho V_s$ used in the SPI modeling of Section 2.3, the other three SPI models without damping or with damping constant of $c = 2\rho V_s$ and $c = 3\rho V_s$ were built to investigate the SPI damping effect on the structure impact responses. All the simulations in this section were conducted under high-energy impact load. As given in Figure 11 of the displacement of cap and pylon top, it can be observed that larger displacements were yielded by the models with smaller c in SPI, which indicated that the incorporation of soil damping will improve the soil resistances for the dynamic impact situation.

As presented in Figure 12, the cap displacement in the soil model without damping was larger than that of the structure model with soil damping. Thus, larger pile displacement by the model without soil damping was obtained rather than other cases as well. Consequently, the bending moment induced by the pile deformation became smaller as the soil damping increased.

4.4. Effect of Axial t-z Spring on the Structural Responses. Normally, the axial SPI is modeled with nonlinear t-z springs placed along the length of the pile. In some cases for simplicity, axial SPI is ignored by replacing the t-z springs as fixed axial degree-of-freedom (DOF) of the pile nodes. To further investigate the influences of axial SPI modeling approach on the impact responses, the models employing axial t-z springs and fixed DOF in axial direction were used to conduct the impact analysis.

Relatively close lateral displacements can be obtained by fixing the axial DOF compared with the SPI model by establishing t-z spring (Figure 13). In addition, the pile lateral displacement with fixed axial DOF at the moment of cap maximum positive displacement was nearly identified with the model with the t-z spring. The pile bending moment by the axial DOF fixed model was slightly larger than that of the model with axial t-z spring (Figure 14). This comparison results demonstrated that fixing the pile DOF in z direction, instead of using t-z spring, is capable of giving reasonable structure results under impact load.

5. Linear Approximation for the *p-y* Soil Curve

The p-y method is commonly recommended in the modeling of SPI for bridge seismic or vessel-substructure impact analysis. While using this approach needs numerical iteration, nonlinear spring element is employed in the analysis, which leads to low computational efficiency and is not convenient in engineering practice as well. In order to overcome these shortcomings, a linear stiffness approximation approach was presented for the SPI modeling in vessel-bridge impact analysis. A flow chart given in Figure 15 illustrates the procedure to get the linear stiffness of soil in each sublayer. A structure model with the p-y soil curve was used to conduct static analysis under maximum impact load P_{max}; thus, the resistance versus lateral displacements of pile node at each elevation along the length can be obtained. Assuming 6 mm is a critical limit to estimate whether the soil is being elastic or inelastic stage [7], different approaches were adopted to linearize the stiffness of soil. For the pile node lateral displacement exceeding 6 mm, the secant stiffness (k_1) in this soil layer was taken as the linear approximation of the soil p-y curve; otherwise, the linear spring attached with the pile node employs initial tangent stiffness of soil p-y curve (k_0) (Figure 16).

Under high-energy vessel impact load, the bridge pylon lateral displacements as well as the pile responses from the models with different SPI considerations were shown in Figures 17 and 18, respectively. The structural responses by the model with tangent soil stiffness were added for the purpose of comparison as well. In Figure 17(a), the cap displacement by the model with soil secant stiffness was larger than the one with the p-y curve (16% larger on the peak value). While the model with k_0 in soil spring yielded smaller cap displacement compared with the p-y curve model. The model with k_1 spring gave relative close prediction on the pylon top lateral displacement rather than a smaller value by the model with k_0 spring.

The pile maximum lateral displacements obtained from the models with k_0 and k_1 springs exhibited either smaller or larger than the p-y model yielding displacement, respectively (Figure 18(a)). It indicates that neither tangent stiffness nor secant stiffness is an appropriate approximation for the soil p-y curve. Adopting tangent stiffness overestimates the soil stiffness while secant stiffness is a bit soft for the SPI modeling. Alternatively, the secant stiffness of soil at 50% maximum lateral pile displacement ($0.5y_c$), denoted as $k_{0.5}$ (Figure 16), was taken as the linear soil stiffness approximation to overcome the shortcoming by utilizing k_0 and k_1 stiffness. As comparisons in Figures 17 and 18, the structure displacements yielded by the $k_{0.5}$ model agreed better with the displacements by the p-y curve than other models with k_0 and k_1 soil stiffness, which demonstrated that the secant stiffness at 50% of y_c was able to give rational responses as an approximation for the nonlinear p-y curve. Despite the pile

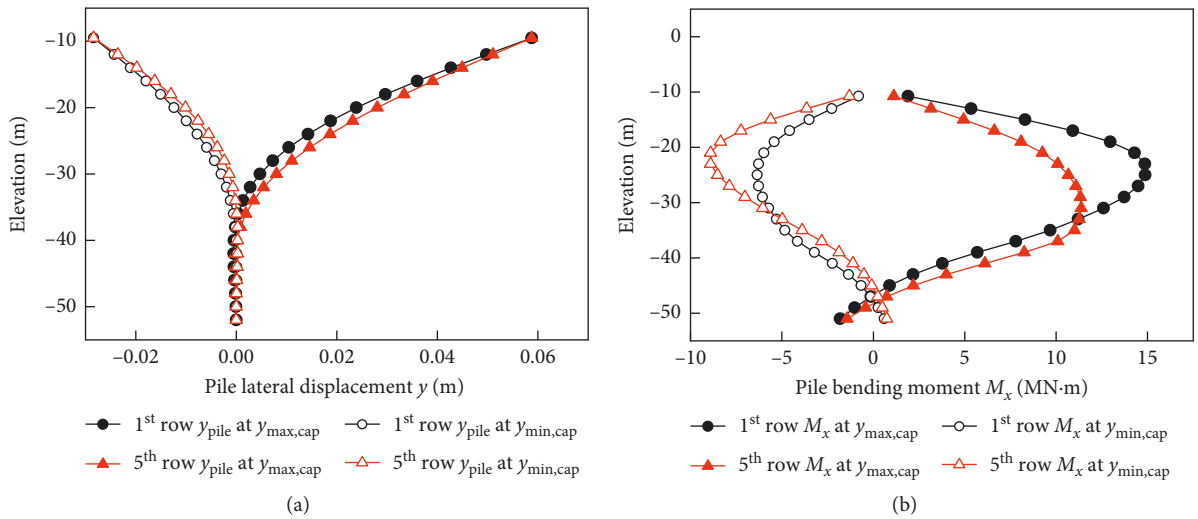

Figure 10: Pile responses in different rows at $y_{max,cap}$ and $y_{min,cap}$. (a) Pile lateral displacement y in 1st and 5th rows. (b) Pile bending moment M_x in 1st and 5th rows.

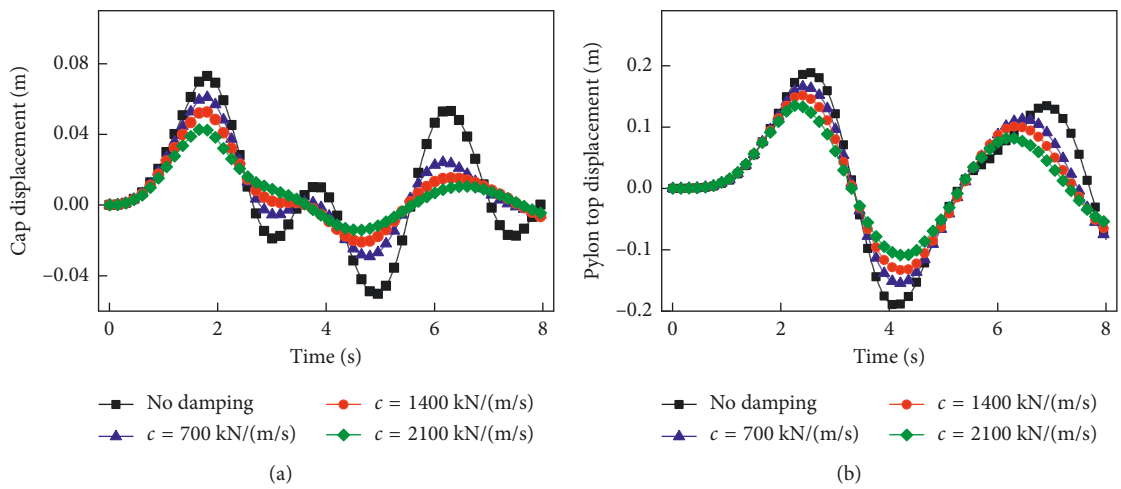

Figure 11: Bridge pylon lateral displacements for various soil damping in SPI. (a) Cap lateral displacement. (b) Pylon top lateral displacement.

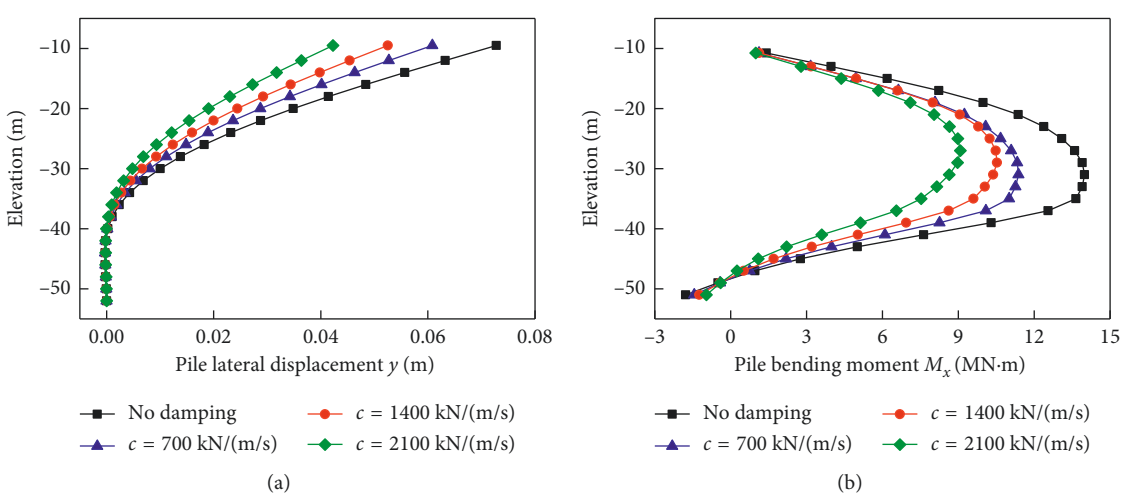

Figure 12: 5th row pile responses for various soil damping. (a) Pile lateral displacement y in the 5th row. (b) Pile bending moment M_x in the 5th row.

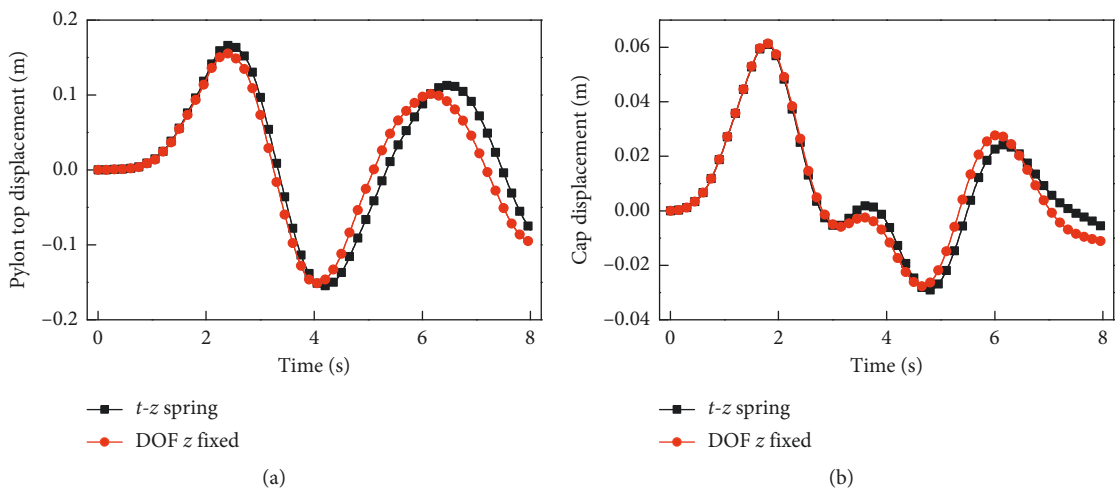

Figure 13: Bridge pylon lateral displacements for different axial SPI considerations. (a) Cap lateral displacement. (b) Pylon top lateral displacement.

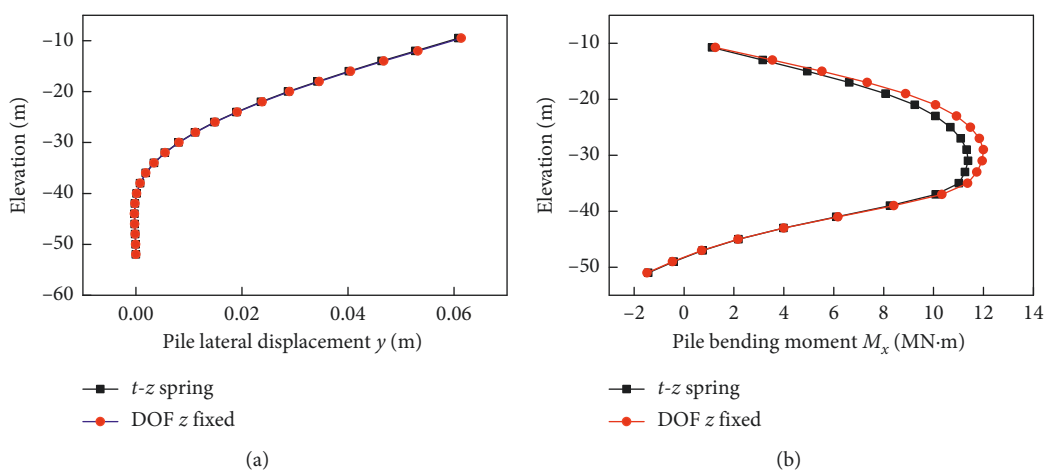

Figure 14: 1st row pile responses for different axial SPI considerations. (a) Pile lateral displacement y in the 5th row. (b) Pile bending moment M_x in the 5th row.

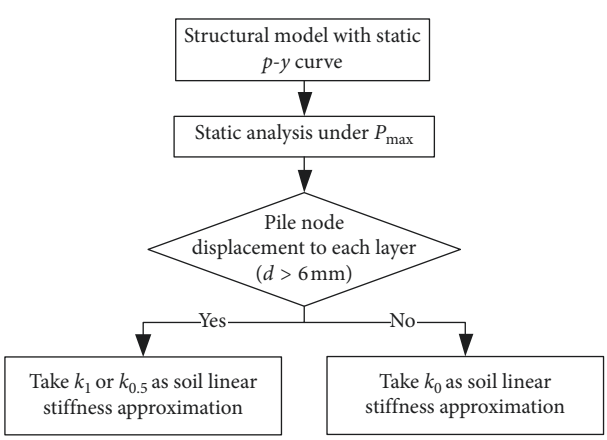

Figure 15: Linear approximation of the soil stiffness.

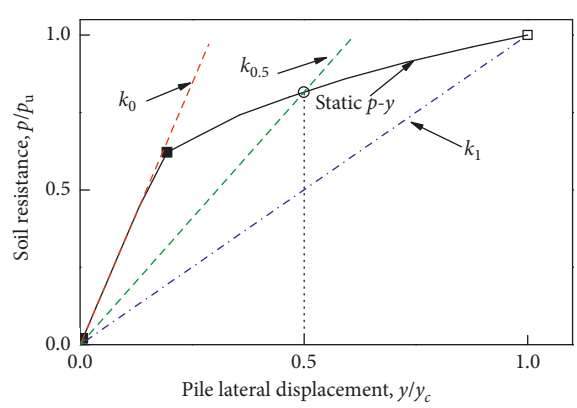

Figure 16: Soil linear stiffness estimation.

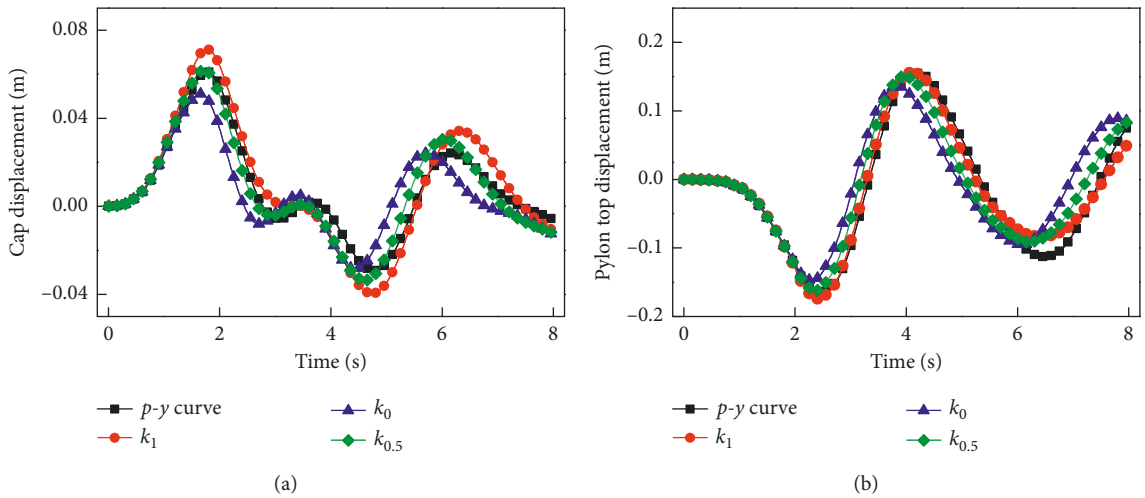

Figure 17: Bridge pylon lateral displacements using different SPI models. (a) Cap lateral displacement. (b) Pylon top lateral displacement.

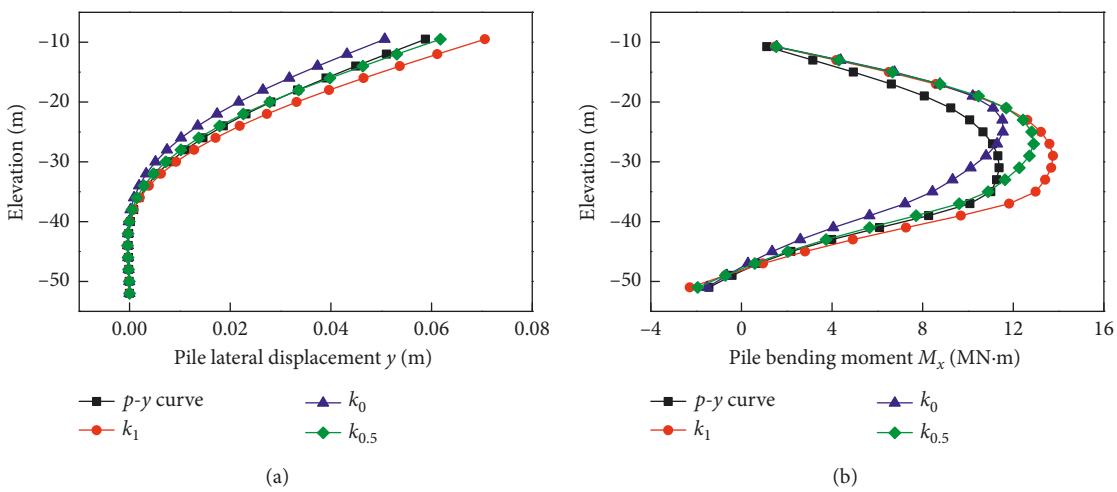

Figure 18: 1st row pile responses by the structure with different SPI models. (a) Pile lateral displacement y in the 5th row. (b) Pile bending moment M_x in the 5th row.

bending moment by soil $k_{0.5}$ model was larger than that of the p-y curve model above −34 m in elevation, it still gave conservative results which tend to be safe for the engineering design.

6. Concluding Remarks

Extensive bridge pylon dynamic analyses were conducted under vessel impact loads. The soil rate-dependent resistance and pile group effect were incorporated into the SPI modeling. The structure and pile responses under the impact load with three various energy levels were compared and discussed, and the influences of pile group effect, soil damping, and axial t-z springs were also investigated. An approximate linear soil stiffness was proposed and validated to replace the p-y curve for engineering application purpose. Several findings and conclusions can be drawn according to the analysis results:

The largest structure and soil responses were achieved under high-energy impact load, and the pile-surrounding soil endured significant inelastic deformation. Moreover, the dynamic soil p-y curve under high (or medium) impact energy increased significantly compared with the static p-y curve. It is necessary to take the soil nonlinearity and rate-dependent effect into the SPI modeling in the structure impact analysis. Since larger p-multiplier was applied in the leading row of the pile group, these piles bore higher proportion lateral load than other piles while smaller displacement was yielded. The incorporation of soil damping would improve the soil resistance, and larger soil damping would yield smaller structure displacement and pile bending moment. Fixing the pile DOF in axial direction, instead of installing t-z springs, was able to give satisfactory predictions on the structural responses. Neither the tangent nor secant stiffness of p-y could be used to replace the nonlinear p-y curve to conduct the structural impact analysis, while the proposed secant stiffness of soil at 50% maximum lateral pile displacement, $k_{0.5}$, was capable of give more reasonable results under vessel impact load.

Data Availability

The data used to support the findings of this study are available from the corresponding author upon request.

Disclosure

The opinions and conclusions do not reflect the views of the funding institutions or other individuals.

Conflicts of Interest

The authors declare that they have no conflicts of interest.

Acknowledgments

This research was supported by the Fundamental Research Funds for the Central Universities, CHD (nos. 310821171004 and 300102219218) and Projects of Natural Science Basic Research of Shaanxi Province, China (2018JQ5093 and 2018JM5018).

References

[1] W. Fan, W. Yuan, and B. Chen, "Steel fender limitations and improvements for bridge protection in ship collisions," *Journal of Bridge Engineering*, vol. 20, no. 12, article 06015004, 2015.

[2] O. D. Larsen, *Ship Collision with Bridges: The Interaction between Vessel Traffic and Bridge Structures*, International Association of Bridge and Structural Engineering, Zürich, Switzerland, 1993.

[3] H. Jiang, J. Wang, M. G. Chorzepa, and J. Zhao, "Numerical investigation of progressive collapse of a multispan continuous bridge subjected to vessel collision," *Journal of Bridge Engineering*, vol. 22, no. 5, article 04017008, 2017.

[4] AASHTO, *Guide Specifications and Commentary for Vessel Collision Design of Highway Bridges*, AASHTO, Washington, DC, USA, 2nd edition, 2009.

[5] CEN (European Committee for Standardization), *Eurocode 1-Actions on Structures, Part 1–7: General Actions-Accidental Actions, EN 1991-1-7:2006*, CEN, London, UK, 2006.

[6] Ministry of Transport of the People's Republic of China, *General Specifications for Design of Highway Bridges and Culverts, JTG D60-2015*, Ministry of Transport of the People's Republic of China, Beijing, China, 2015.

[7] Ministry of Transport of the People's Republic of China, *Code for Design on Subsoil and Foundation of Railway Bridge and Culverts, TB 10002.5-2005*, Ministry of Transport of the People's Republic of China, Beijing, China, 2005.

[8] M. T. Davidson, G. R. Consolazio, and D. J. Getter, "Dynamic amplification of pier column internal forces due to barge-bridge collision," *Transportation Research Record: Journal of the Transportation Research Board*, vol. 2172, no. 1, pp. 11–22, 2010.

[9] W. Fan, W. Yuan, Z. Yang, and Q. Fan, "Dynamic demand of bridge structure subjected to vessel impact using simplified interaction model," *Journal of Bridge Engineering*, vol. 16, no. 1, pp. 117–126, 2011.

[10] P. Yuan and I. E. Harik, "Equivalent barge and flotilla impact forces on bridge piers," *Journal of Bridge Engineering*, vol. 15, no. 5, pp. 523–532, 2010.

[11] G. R. Consolazio, R. A. Cook, and M. C. McVay, *Barge Impact Testing of the St. George Island Causeway Bridge*, Engineering and Industrial Experiment Station, University of Florida, Gainesville, FL, USA, 2006.

[12] J. Zhang, X. Chen, D. Liu, and X. Li, "Analysis of bridge response to barge collision: refined impact force models and some new insights," *Advances in Structural Engineering*, vol. 19, no. 8, pp. 1224–1244, 2016.

[13] Y. E. Mostafa and M. H. E. Naggar, "Dynamic analysis of laterally loaded pile groups in sand and clay," *Canadian Geotechnical Journal*, vol. 39, no. 6, pp. 1358–1383, 2002.

[14] Z. Y. Ai, Z. X. Li, and L. H. Wang, "Dynamic response of a laterally loaded fixed-head pile group in a transversely isotropic multilayered half-space," *Journal of Sound and Vibration*, vol. 385, pp. 171–183, 2016.

[15] G. Anoyatis, G. Mylonakis, and A. Lemnitzer, "Soil reaction to lateral harmonic pile motion," *Soil Dynamics and Earthquake Engineering*, vol. 87, pp. 164–179, 2016.

[16] W. Fan and W. C. Yuan, "Numerical simulation and analytical modeling of pile-supported structures subjected to ship collisions including soil-structure interaction," *Ocean Engineering*, vol. 91, pp. 11–27, 2014.

[17] A. Taha, M. Hesham El Naggar, and A. Turan, "Numerical modeling of the dynamic lateral behavior of geosynthetics-reinforced pile foundation system," *Soil Dynamics and Earthquake Engineering*, vol. 77, pp. 254–266, 2015.

[18] Ministry of Transport of the People's Republic of China, *Code for Design of Ground Base and Foundation of Highway Bridges and Culverts, JTG D63-2007*, Beijing, China, 2007.

[19] M. McVay, S. Wasman, and P. Bullock, *Barge Impact Testing of St. George Causeway Bridge Geotechnical Investigation*, Department of Civil and Coastal Engineering, University of Florida, Gainesville, FL, USA, 2005.

[20] L. C. Reese, W. R. Cox, and F. D. Koop, "Analysis of laterally loaded piles in sand, Paper No. OTC 2080," in *Proceedings of the Fifth Annual Offshore Technology Conference*, Houston, TX, USA, May 1974.

[21] S. T. Wang and L. C. Reese, *COM624P-Laterally Loaded Pile Analysis for Microcomputer, ver.2.0, FHWA-SA-91-048*, FHWA, Springfield, VA, USA, 1993.

[22] H. Matlock, *Correlations for Design of Laterally Loaded Piles in Soft Clay*, Offshore Technology Conference, Dallas, TX, USA, 1970.

[23] M. C. McVay and L. Niraula, "Development of modified t-z curves for large diameter piles/drilled shaft in limestone for FB-Pier," Report No. 4910-4504-878-12, National Technical Information Service, Springfield, VA, USA, 2004.

[24] G. Gazetas and R. Dobry, "Simple radiation damping model for piles and footings," *Journal of Engineering Mechanics*, vol. 110, no. 6, pp. 937–956, 1984.

[25] AASHTO, *AASHTO LRFD Bridge Design Specifications*, AASHTO, Washington, DC, USA, 5th edition, 2010.

[26] LSTC (Livermore Software Technology Corporation), *LS-DYNA Theory Manual*, LSTC, Livermore, CA, USA, 2006.